Bulletin of the JSME Vol.000,No.00,2013
Mechanical Engineering Journal

Properties of the laminar-turbulent transition in a mixing layer by the low-frequency disturbance (Effect of the anti-symmetrical disturbance)

Masashi ICHIMIYA*, Hiroshi SAKAI** and Takeshi OOHARA**
* Department of Mechanical Engineering, The University of Tokushima
2-1 Minami-Josanjima-cho, Tokushima-shi, Tokushima, 770-8506, Japan
E-mail: ichimiya@tokushima-u.ac.jp
** Graduate School, The University of Tokushima
2-1 Minami-Josanjima-cho, Tokushima-shi, Tokushima, 770-8506, Japan

Received 17 December 2013

Abstract
The laminar-turbulent transition of a mixing layer excited by oscillating flat plates at an exit of a two-dimensional nozzle was experimentally investigated. The mixing layer was formed between the jet issued from the nozzle and the surrounding quiescent fluid. The plates oscillated vertically in relation to the mean flow. Upper and lower flat plates oscillated anti-symmetrically. The oscillation frequency, 5 Hz, was two orders of magnitude smaller than the fundamental frequency of the velocity fluctuation in the natural transition process. Mean and fluctuating velocity components in the streamwise and normal directions were measured by hot-wire anemometers. The results were compared with the previous case in which the plates oscillated symmetrically. Anti-symmetrical oscillation promoted the expansion of the mixing layer and promoted the disappearance of the potential core more than symmetrical oscillation. The periodic motion of the flow promotes the fluctuation from the time-averaged velocity. The fluctuations from time and phase averages in the anti-symmetrical oscillation were larger than those in the symmetrical oscillation. The contribution of periodic fluctuation disappeared downstream in the symmetrical oscillation but persisted longer in the anti-symmetrical oscillation. In the linear region of the transition, the irregular fluctuation grew exponentially. There were not any differences in the spatial growth rate between the streamwise and normal directions and among three oscillating states. In the nonlinear region, factors other than the temporal fluctuation energy convection and production rates may contribute to the increase in velocity temporal fluctuation in the streamwise component. On the other hand, the convection and production rates may contribute to the increase in velocity fluctuation in the normal component there.

Key words : Mixing layer, Transition, Turbulence, Jet, Shear flow, Oscillating plate, Periodic disturbance

1. Introduction

The laminar-turbulent transition phenomenon has been investigated for many years, because it occurs very often in the natural world and in the industrial machinery field. The transition in free shear flow is also an important issue. Many kinds of free shear flow have been shown (Rajaratnam, 1976)(Shakouchi, 2004). One example is a mixing layer formed between the jet just behind a nozzle and the surrounding quiescent fluid. This type of mixing layer is classified as a ‘jet boundary’ in Schlichting and Gersten (2000). The present study concerns the laminar-turbulent transition in the mixing layer as one of the fundamental problems in the transition in free shear flow.

In many previous experiments, disturbances were forced from outside onto the laminar mixing layer. In the early stage of the forced disturbances, the excitation frequency was set equal to the fundamental frequency of the velocity fluctuation in the linear region of the unforced, i.e., natural transition process. Though the mixing layer is unstable under disturbances with a low wave number, i.e., a long wavelength in contrast with the boundary layer, the transition

Received xx December 2013 (No.xx-xxxx)
[DOI: 00.0000/ABCDE0.0000000]

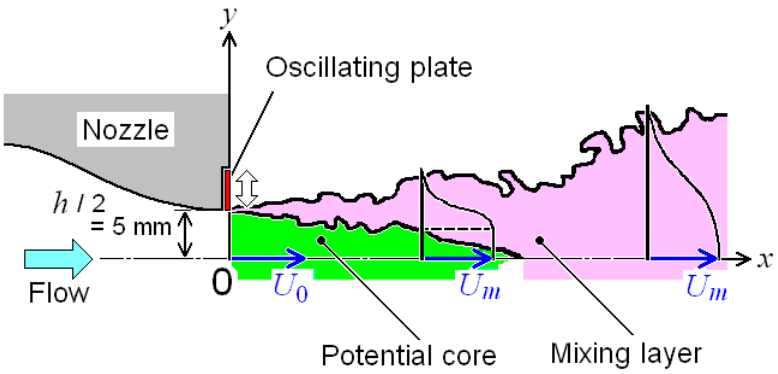

Fig. 1 Schematic diagram of two-dimensional mixing layer and coordinate system. Velocity profiles in the figure show the ones where the vertical lines exist.

process with a periodic disturbance with a long wavelength has not been investigated. Two kinds of sinusoidal velocity fluctuation are found in the region where laminar jet becomes unstable; one is symmetrical and the other is anti-symmetrical with respect to the centerline of the jet (Sato, 1960). Makita et al. (1988) excited the velocity disturbances by the sound wave speed and clarified the difference of the two modes.

In the present study the disturbances were caused by thin plate oscillation perpendicular to the stream at a low frequency. The effect of the disturbance on the laminar-turbulent transition of the mixed layer is experimentally investigated. So far, two kinds of experiments were conducted; in one, the plates at the nozzle exit do not protrude into the nozzle section and remain in a 'stationary state'; and in the other, 'symmetrical oscillating state' plates oscillate perpendicularly to the flow and symmetrically with each other in relation to the flow (Ichimiya, et al., 2011, 2013a, 2013b). In the previous paper (Ichimiya, et al., 2013b), effects of the oscillation frequency and amplitude were examined. In the present study, the two plates oscillate anti-symmetrically with respect to the centerline, and then the mixing layer moves periodically. The effect of the periodic motion is compared with the previous two states.

2. Experimental apparatus and measurement methods

A blowing-type wind tunnel was used in which air is blown into the measurement section from a two-dimensional nozzle exit of aspect ratio 31 (310 mm in width and 10 mm in height, h). Moreover, a ceiling wall was installed whose height from the nozzle centerline is equal to the vertical distance between the centerline and the floor. Mean velocity profiles were measured at some spanwise positions downstream of the nozzle, and they coincided well with each other.

The upper half of the flow field and coordinate system are shown in Fig. 1. The coordinate origin is at the center of the nozzle exit section. The x- and y-axis are the streamwise and cross-stream directions, respectively.

Two oscillation plates 2 mm in thickness were equipped across the whole width to make a disturbance in the upper and lower mixing layer. The plates oscillate perpendicularly and sinusoidally in relation to the flow at a frequency of 5 Hz. The low frequency, 5 Hz, adopted in the present study is two orders of magnitude lower than the common fundamental frequency of several hundred Hz, which is observed in the early stage of many experiments (Sato, 1960)(Huang and Ho, 1990). Moreover, it is also smaller than the frequency of the coherent structure in the mixing layer of a few hundred or thousand Hz (Brown and Roshko, 1974)(Moore, 1977). The distribution of fluctuating vorticity in such a long wavelength, i.e., the process during large eddy changes into a smaller eddy which exists in turbulent flow, has not been investigated thoroughly. Therefore, studies which can cover a wide range of wavelength corresponding to that of the fluctuating vorticity are awaited. The problems with low frequency disturbance are expected to be solved also in the industrial world, for example, in an air oscillation whose frequency is less than audio frequency. The bottom of the oscillating plate in Fig. 1 becomes flush with the nozzle wall surface when it rises to its highest point, and then descends from the surface by 0.5 mm at most. Another plate is installed at the lower half of the flow field. Both plates oscillate anti-symmetrically with respect to the nozzle centerline (y = 0), 'anti-symmetrical oscillating state'. Therefore, the nozzle exit height, h, of 10 mm, is always narrowed 0.5 mm. In the present investigation, the anti-symmetrical oscillating state is compared with the previous stationary state and symmetrical oscillating state.

The Reynolds number was 5000 based on the nozzle exit velocity without oscillation, $U_0 \simeq$ 7.5 m/s, and nozzle

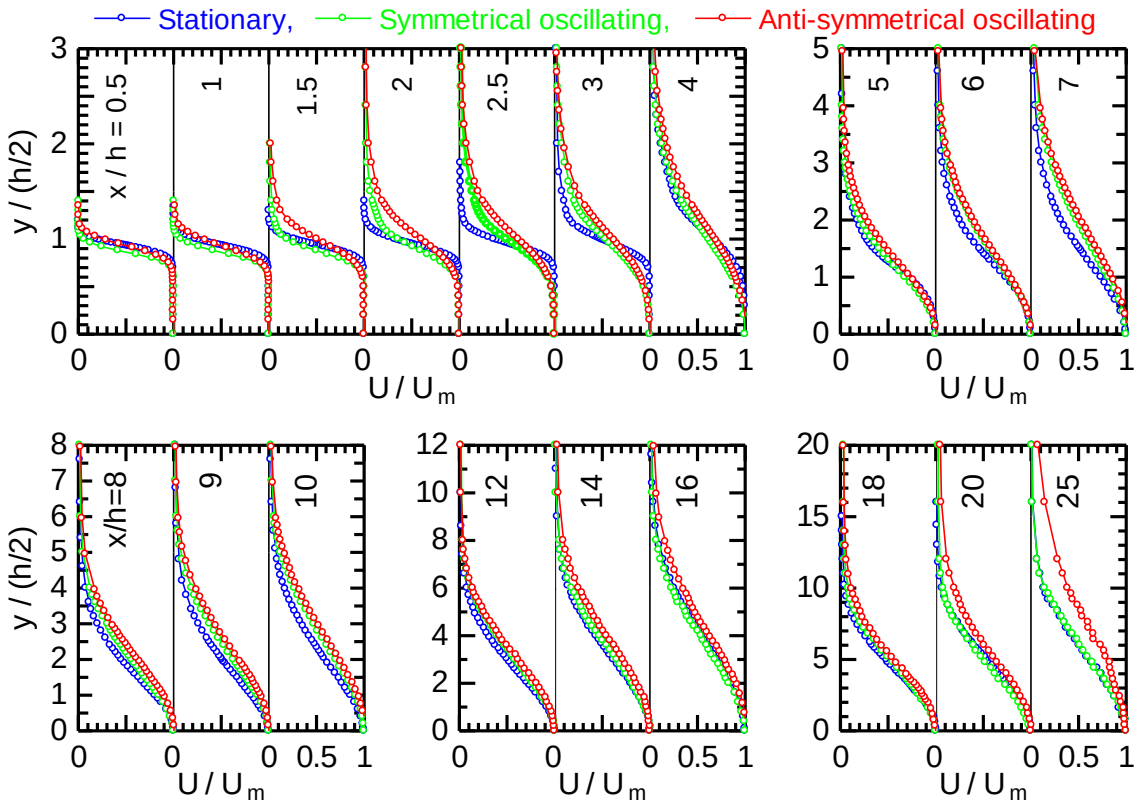

Fig. 2 Mean velocity profiles

exit height, h. X-shaped hot-wire probes with two tungsten sensing elements, each 5 μm in diameter and 1 mm in length, were used for the measurements. Output voltage was sampled at a frequency of 5 and 10 kHz for about 26 and 52 seconds in the stationary and both oscillating states, respectively. This interval is equivalent to about 260 oscillations when the plates oscillate.

3. Results and discussion

3.1 Mean velocity and expansion of mixing layer

Figure 2 shows the mean velocity profiles of the streamwise component. Here, the time-averaged velocity, U, is normalized by the velocity on the local centerline, U_m, and the normal distance from the centerline, y, is normalized by the half-height of the nozzle exit, $h/2$ = 5 mm. Just behind the nozzle, the potential core region where the velocity is constant is wide. On the other hand, the mixing layer where the velocity gradient exists is quite narrow. Farther downstream the potential core gradually becomes narrower and the mixing layer becomes wider. The potential core region persists in the region of $x/h \leqq 3$, 2.5 and 2 in the stationary, symmetrical oscillating and anti-symmetrical oscillating states, respectively. Thus, the disappearance of the potential core is promoted by the low-frequency disturbance due to the oscillating plates and is more promoted by the anti-symmetrical disturbance.

Next, the expansion of the mixing layer is considered. Figure 3 shows the streamwise variation of the centerline velocity. The velocity is normalized by the nozzle exit velocity without plate oscillation. In all states, the velocity is almost constant first, then it decreases downstream. In the symmetrical oscillating state, the nozzle exit area decreases periodically due to the oscillating plates. Therefore, in the region of $x/h \leqq 3$, the centerline velocity, U_m, is larger than the nozzle exit velocity without plate displacements within the nozzle, U_0. On the other hand, in the anti-symmetrical oscillating state, the nozzle exit area is kept constant regardless of the plate oscillation phase. Therefore, the centerline velocity is the same as the nozzle exit velocity. As a guide for the streamwise decrease, stations where the velocity divided by itself at x/h = 0.5 decreases to 0.98 are x/h = 5, 4.2 and 3.3 for the stationary, symmetrical oscillating and anti-symmetrical oscillating states, respectively. That is, the decrease is promoted by the plate oscillation and it is further promoted by the anti-symmetrical oscillation. The final values downstream are the same for the stationary and symmetrical oscillating states, however, it for the anti-symmetrical oscillating state is smaller than the other states.

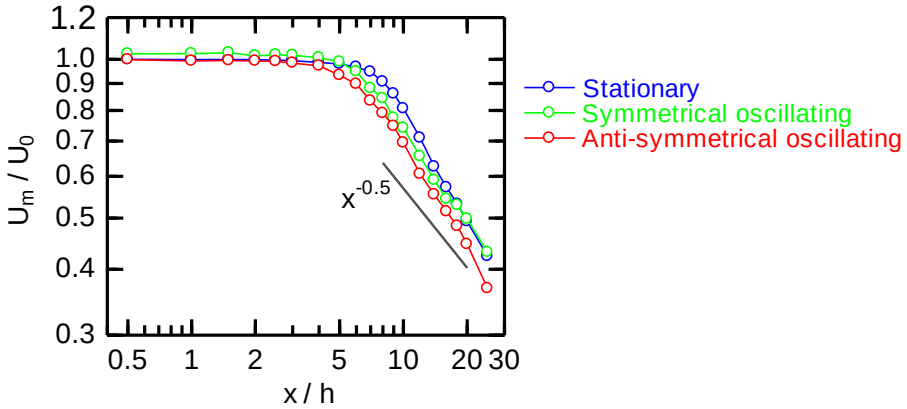

Fig. 3 Streamwise variation of centerline velocity

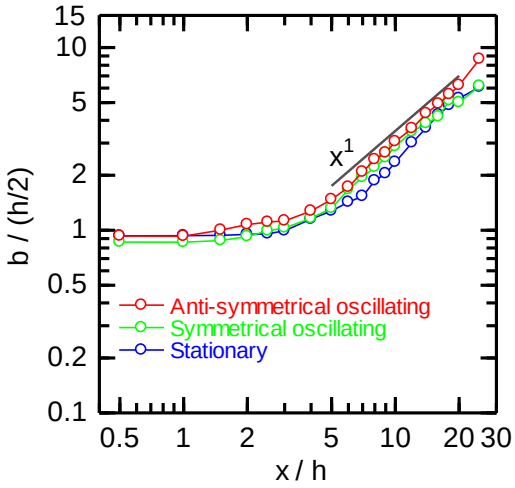

Fig. 4 Streamwise variation of half-width

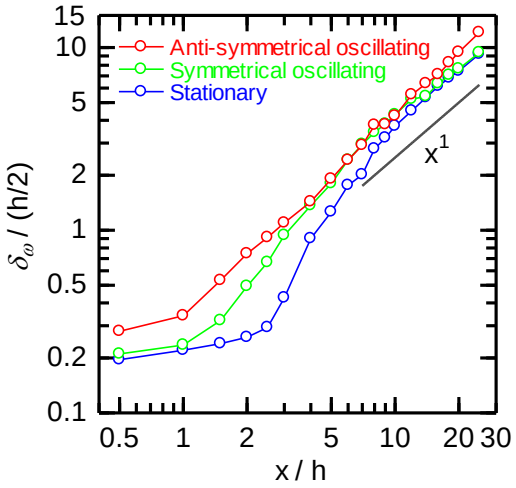

Fig. 5 Streamwise variation of vorticity thickness

Figure 4 shows the streamwise variation of the half-width. As stated above, in the region of $x/h \leqq 3$, the half-width in the symmetrical oscillating state is smaller than that in the stationary state due to the displacement of the oscillating plates within the nozzle. In the anti-symmetrical oscillating state, though the displacement is the same as the symmetrical oscillating state, the half-width is larger than that in the symmetrical oscillating state. The strong diffusion of the mixing layer due to the periodic change of the jet induced by the oscillation of the constant area of the jet in the cross-jet direction may contribute to enlarge the half-width. The half-width increases downstream. The streamwise stations of the start of the increase are x/h = 3, 1.5 and 1, respectively. Therefore, the diffusion effect in the anti-symmetrical oscillating state is the strongest. Downstream, the final value in the anti-symmetrical oscillating state is larger than the other states.

Figure 5 shows the streamwise variation of the vorticity thickness, $\delta_\omega = -U_m / (\partial U/\partial y)_{max}$, where $(\partial U/\partial y)_{max}$ is the maximum value in the mean velocity gradient at a local x/h. In the region of $x/h \leqq 5$ the mixing layer is wider in the anti-symmetrical oscillating state than the symmetrical oscillating and stationary states. Downstream, the difference of the expansion of the mixing layer between in both oscillating states becomes smaller, though the mixing layer in the anti-symmetrical oscillating state is wider than that in the symmetrical oscillating state finally due to the periodic motion.

3.2 Fluctuating velocity

In this section two kinds of fluctuating velocity components are shown. One is obtained from a time-averaged velocity, then root mean square values of the fluctuating velocity u' and v' are obtained finally. The other kind is obtained from a phase-averaged velocity at 100 phases, the square of the deviations from the phase-averaged velocity are phase averaged again, and then the square root u^* and v^* are also finally obtained (Ichimiya, et al., 2013b). Maximum values in the distribution for the y-direction at the respective station, x/h, are chosen as their representatives.

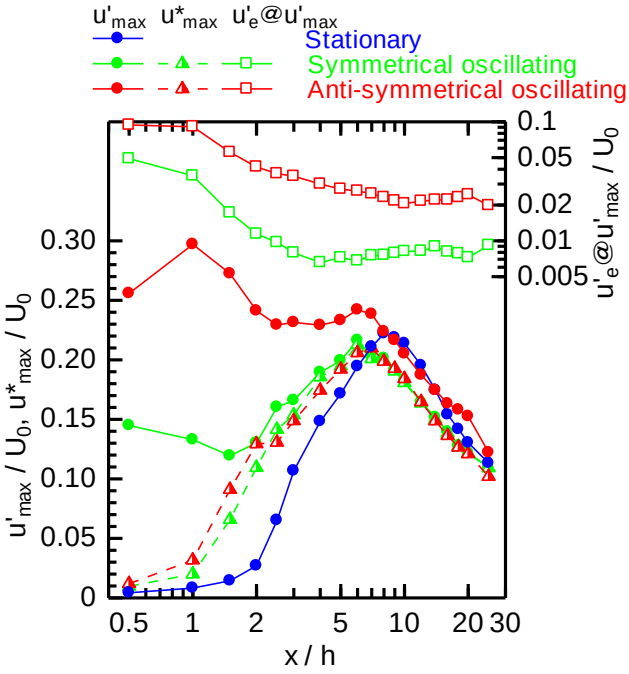

Fig. 6 Streamwise variation of maximum fluctuating velocities in the streamwise component

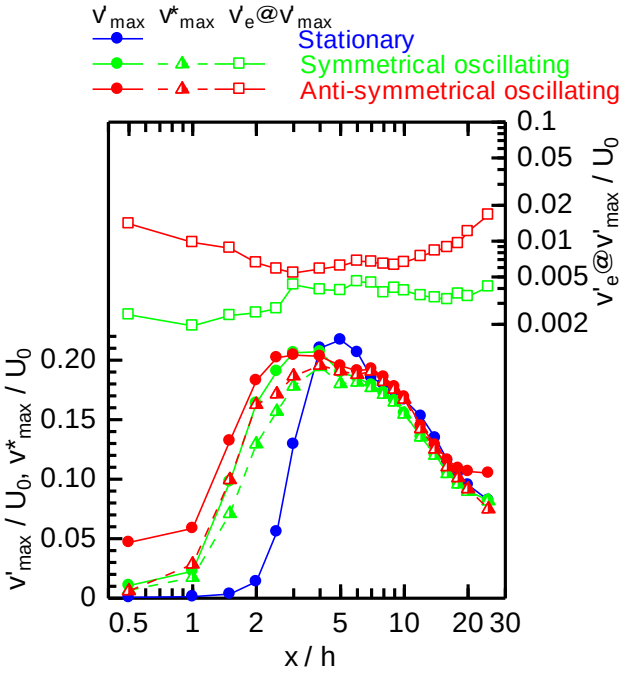

Fig. 7 Streamwise variation of maximum fluctuating velocities in the normal component

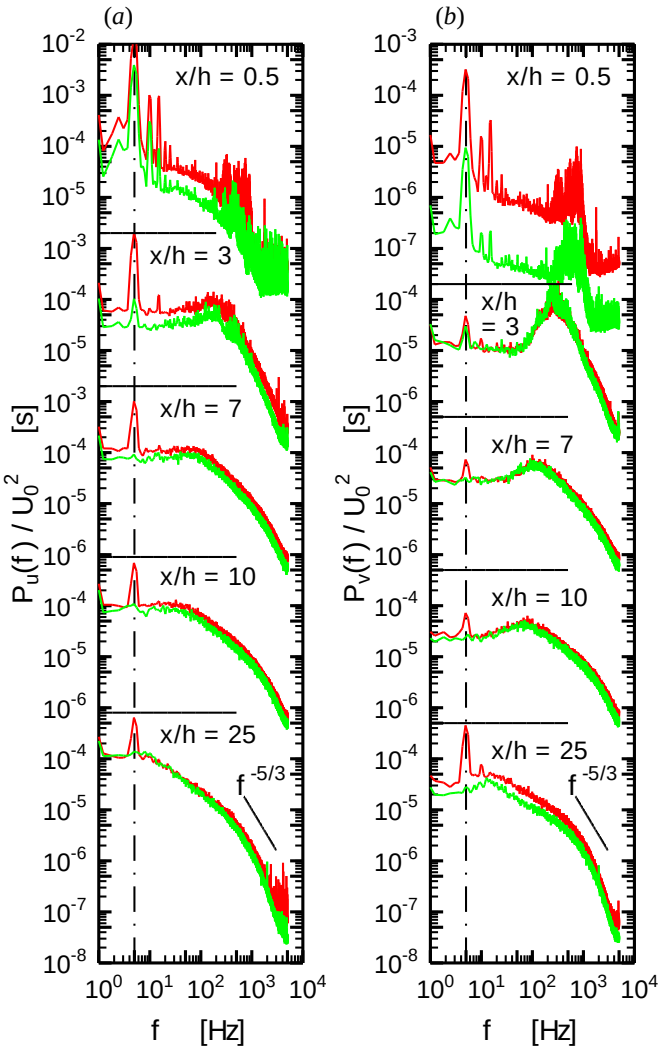

Fig. 8 Power spectrum density function of temporal fluctuating velocity in (*a*) streamwise and (*b*) normal components. green line, symmetrical oscillating state; red line, anti-symmetrical oscillating state.

The *y*-positions where the fluctuating velocities reach the maximum are almost same as the half-width, Fig. 4, while the potential core exists. Downstream, the positions gradually shift toward the inside of the half-width. At x/h = 25, the positions are approximately 60% of the half-width in all oscillating cases. The streamwise components u'_{max} and u^*_{max} are shown in Fig. 6. The normal components v'_{max} and v^*_{max} are shown in Fig. 7. The velocities are normalized by the nozzle exit velocity, U_0.

At first, the streamwise component in Fig. 6, is considered. If the distribution of u'_{max} in the stationary state is shifted upstream, it almost corresponds to that in the symmetrical oscillating state except for the region of $x/h \leqq 2$. Therefore, the plate oscillation promotes the streamwise variation of the fluctuation from the time average. However,

the value of u'_{max} in the anti-symmetrical oscillating state is larger than that in the symmetrical oscillating state at the respective streamwise station. At first, the fluctuation in the stationary state increases monotonically, though in both oscillating states they take fairly large values at x/h = 0.5 and 1 at symmetrical and anti-symmetrical oscillating states, respectively, before decreasing rapidly.

The fluctuation from the phase-averaged velocity, u^*_{max}, is almost the same between both oscillating states. Therefore, in the anti-symmetrical oscillating state, the difference $u'_{max} - u^*_{max}$, i.e., the contribution from the periodic variation by the oscillating plates is larger than in the symmetrical oscillating state. The contribution persists even at x/h = 25. This fact is recognized from a power spectrum density of the temporally fluctuating velocity. In Fig. 8, the power spectrum density functions of the fluctuating velocities, u and v, are shown at five streamwise stations. The spectrum density, $P_u(f)$ and $P_v(f)$, are shown at y-positions where the rms values based on the time average, u' and v', becomes maximum at the each station, respectively. They take peak at the oscillating frequency, 5 Hz. The spectrum function at the oscillation frequency was multiplied by the step of frequency in the spectrum calculation, then its square root, u_e', was obtained (Ichimiya, et al., 2013b). It corresponds to the contribution of the oscillation frequency to the root mean square value of the temporally fluctuating velocity, u'. Therefore, it expresses the periodic fluctuation with the plate oscillation. The streamwise variation of the value where the time-averaged rms value takes maximum at a local x/h is also shown in Fig. 6. Though the periodic fluctuations, u_e', are large at x/h = 0.5 and 1, they decrease downstream. The value in the anti-symmetrical oscillating state is larger than that in the symmetrical oscillating state. Therefore, the periodic motion of the jet causes the large periodic velocity fluctuation just behind the nozzle.

Next, the normal component in Fig. 7, is considered. The fluctuations from the time-averaged velocity, v'_{max}, increase monotonically until x/h = 5, 3 and 3 in the stationary, symmetrically and anti-symmetrically oscillating states, respectively. These stations almost correspond to where the potential core region disappears in the respective state. Downstream the fluctuations decrease. Therefore, in the region where the potential core persists and becomes narrower, the fluctuation increases. Once the potential core disappears, both mixing layers that have existed on both sides of the potential core merge, and the fluctuation may then distribute within the wide mixing layer and decrease.

As in the streamwise component, Fig. 6, the oscillating plate disturbance enhances the streamwise variation in the normal temporally fluctuating velocity, v'_{max}. In addition, the value in the anti-symmetrical oscillation state is larger than that in the symmetrical oscillation state as a whole. Especially, just behind the nozzle, $x/h \leqq 1$, the difference of values between both oscillating states is larger due to the large periodic variation by the oscillating plates. Additionally, downstream, $18 \leqq x/h$ also, the difference is larger due to the periodic motion of the jet. The difference $v'_{max} - v^*_{max}$, i.e., the contribution from the periodic variation, is larger in the anti-symmetrical oscillating state in the region of $x/h \leqq 2$ and downstream, $10 \leqq x/h$. The difference persists even at x/h = 25. The fact is also seen from the periodic fluctuation, v_e'. In the anti-symmetrical oscillating state, first it decreases, then it increases downstream due to the periodic motion of the jet and finally it takes approximately same value as that at x/h = 0.5.

Figure 9 shows the streamwise variation of the maximum value of the Reynolds shear stress component. If the distribution of $\overline{uv}_{max}$ in the stationary state is shifted upstream, it almost corresponds to that in the symmetrical

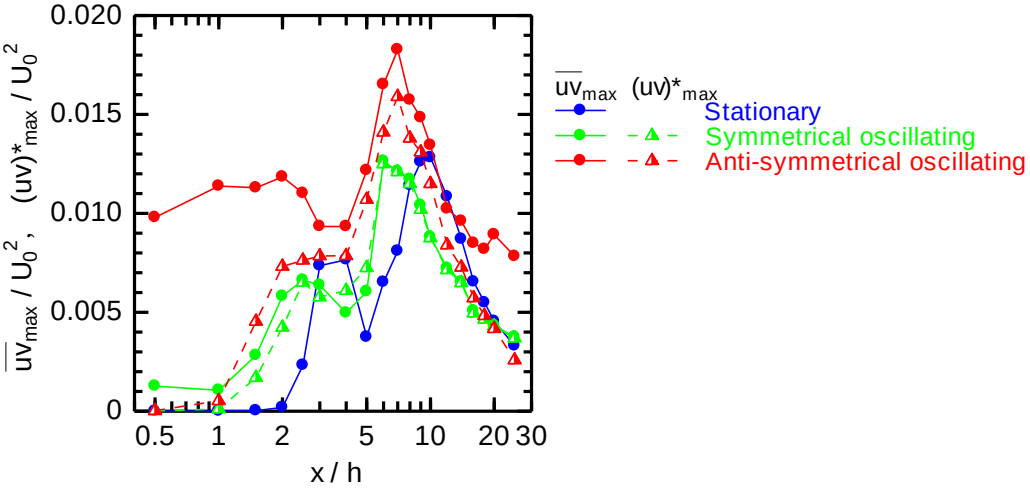

Fig. 9 Streamwise variation of Reynolds shear stress component

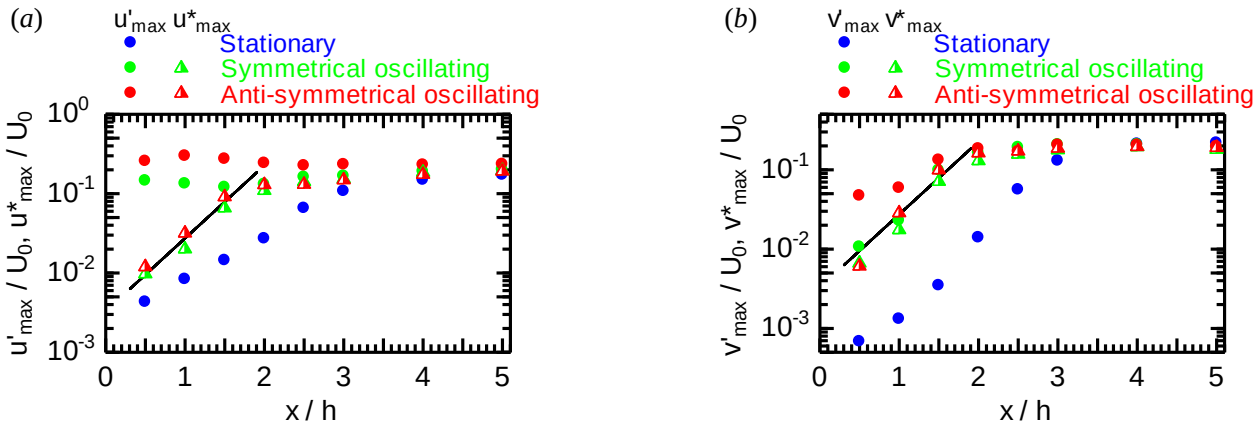

Fig. 10 Growth rate of fluctuating velocities in (*a*) streamwise and (*b*) normal components.

oscillating state. In addition, if the value in the symmetrical oscillating state is magnified, it almost corresponds to that in the anti-symmetrical oscillating state except for $x/h < 2$. The large value there in the anti-symmetrical oscillating state may be due to the large periodic fluctuation in the streamwise fluctuating velocity, u'_{max}, in Fig. 6. After $x/h = 4$, 2.5 and 2 in the stationary, symmetrical oscillating and anti-symmetrical oscillating states, respectively, they decrease due to the decrease of the production rate, Fig. 15. The second increase is due to the increase of the streamwise and normal fluctuating velocities, Figs. 6 and 7. In Fig. 9 an irregularly fluctuating component of the Reynolds shear stress, $(uv)^*$, is also shown. This is a difference of a phase-average of a product of instantaneous streamwise and normal velocities, $<\tilde{u}\tilde{v}>(\tau)$, and a product of phase-averaged instantaneous velocities, $<\tilde{u}>(\tau)<\tilde{v}>(\tau)$, i.e.,

$$\begin{aligned} &<\tilde{u}\tilde{v}>(\tau) - <\tilde{u}>(\tau)<\tilde{v}>(\tau) = <(U+u)(V+v)>(\tau) - <U+u>(\tau)\,<V+v>(\tau) \\ &= [UV + U<v>(\tau) + V<u>(\tau) + <uv>(\tau)] - [UV + U<v>(\tau) + V<u>(\tau) + <u>(\tau)\,<v>(\tau)] \\ &= <uv>(\tau) - <u>(\tau)\,<v>(\tau) \end{aligned} \tag{1}$$

where τ ($0 \leqq \tau < 1$) is the phase of the oscillation, $\tilde{u}$ and $\tilde{v}$ are instantaneous velocities, U and V are time-averaged velocities, and u and v are fluctuating velocities from the time-averaged ones. Next, they are phase averaged over 100 phases, and then the final value, $(uv)^*$, is obtained. The irregular Reynolds shear stress in the anti-symmetrical oscillating state is almost larger that in the symmetrical oscillating state.

A spatial growth rate of the fluctuating velocities is considered from gradients in their semi-log plots in Fig. 10. The straight lines in Fig. 10 show maximum spatial growth rate according to the spatial stability theory of Michalke (1965). Details for the estimation of the spatial growth rate was described in Ichimiya (2013b). In the stationary state the time-averaged fluctuations, u'_{max} and v'_{max} collapse on the straight line, i.e., they grow exponentially. On the other hand, in the symmetrical oscillating state the irregular fluctuations, u^*_{max} and v^*_{max} grow exponentially. In the anti-symmetrical oscillating state also, the irregular fluctuations grow exponentially. The linear region where the irregular fluctuation grows exponentially in the streamwise direction is the region where $x/h \leqq 3$ and 1.5 in the stationary and both oscillating states, respectively. There are not any differences in the spatial growth rate between the streamwise and normal directions and among three oscillating states.

3.3 Fluctuation energy

Near the end of the linear region the temporally fluctuating velocity reaches a fairly large value as seen in Figs. 6 and 7. Therefore, the temporal fluctuation energy convection and production rates due to the second-power term of the temporal fluctuation velocity may be critical even in the linear region. The boundary-layer-approximated temporal fluctuation energy budget and Reynolds shear stress equations are (Rotta, 1962):

$$U\frac{\partial}{\partial x}\frac{\overline{u^2}}{2} + V\frac{\partial}{\partial y}\frac{\overline{u^2}}{2} = -\overline{u^2}\frac{\partial U}{\partial x} - \overline{uv}\frac{\partial U}{\partial y} + \frac{1}{\rho}\overline{p\frac{\partial u}{\partial x}} - \frac{\partial}{\partial y}\frac{\overline{u^2 v}}{2} + \nu\overline{u\nabla^2 u} \tag{2}$$

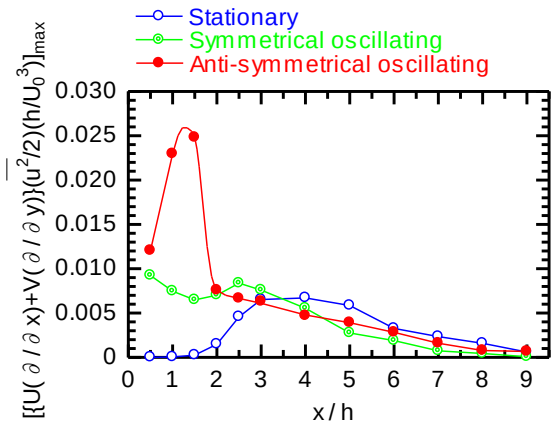

Fig. 11 Streamwise variation of maximum values of temporal fluctuation energy convection rates in the streamwise component

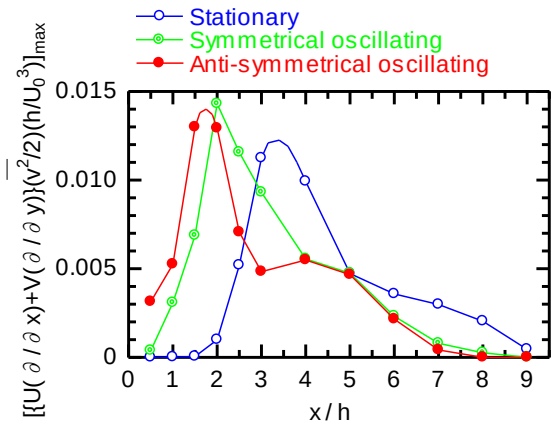

Fig. 12 Streamwise variation of maximum values of temporal fluctuation energy convection rates in the normal component

$$U\frac{\partial}{\partial x}\frac{\overline{v^2}}{2}+V\frac{\partial}{\partial y}\frac{\overline{v^2}}{2}=-\overline{v^2}\frac{\partial V}{\partial y}+\frac{1}{\rho}\overline{p\frac{\partial v}{\partial y}}-\frac{\partial}{\partial y}\frac{\overline{v^3}}{2}-\frac{\partial}{\partial y}\frac{\overline{vp}}{\rho}+\nu\overline{v\nabla^2 v} \tag{3}$$

$$U\frac{\partial\overline{uv}}{\partial x}+V\frac{\partial\overline{uv}}{\partial y}=-\overline{v^2}\frac{\partial U}{\partial y}+\frac{1}{\rho}\overline{p\left(\frac{\partial u}{\partial y}+\frac{\partial v}{\partial x}\right)}-\frac{\partial}{\partial y}\left(\overline{uv^2}+\frac{\overline{up}}{\rho}\right)+\nu\left(\overline{v\nabla^2 u}+\overline{u\nabla^2 v}\right). \tag{4}$$

The temporal fluctuation energy convection rate in Eq. (2) and (3), and production rate in the three equations are discussed. For further discussion about the transition, the energy and Reynolds shear stress of the irregular fluctuation are more desirable to consider. To obtain the derivative of the velocity, the linear gradient of the two velocities at the two measuring points was calculated. Then, the gradient was regarded as the derivative of the middle point between the two points.

First, the fluctuation energy convection rate is considered. The maximum values of the convection rate in the distribution in *y*-direction of the $\overline{u^2}/2$ and $\overline{v^2}/2$ are shown in Figs. 11 and 12, respectively. They will be compared with the temporally fluctuating velocities in Figs. 6 and 7 to estimate contributions of the convection rate to the temporally fluctuating velocity.

First, the streamwise components in Figs. 6 and 11 are compared. As mentioned before in Fig. 6, the oscillating plate disturbance promotes the streamwise variation of the fluctuating velocity, though the mode of oscillation does not. In Fig. 11, the streamwise variation of the convection rate in both oscillating states appears more upstream than the stationary state. The convection rate in the stationary state also increases in the *x*-direction monotonically, though in the anti-symmetrical oscillating state it takes fairly large value in the region of $x/h \leqq 1.5$, then decreases rapidly. Therefore, the streamwise variation process of the convection rate corresponds to that of the fluctuating velocity. In the linear region the stations where the convection rates begin to decrease are x/h = 4, 2.5 and 1.5 in the stationary, symmetrical and anti-symmetrical oscillating states, respectively.

Next, the normal components in Figs. 7 and 12 are compared. In Fig. 12, the streamwise variation of the convection rate in both oscillating states appears more upstream than the stationary state. The difference of the variation in both oscillating states is small. In addition, as the fluctuating velocity, in the region of $x/h \leqq 1.5$, the value in the anti-symmetrical oscillating state is larger than that in the symmetrical oscillation state. Therefore, also in the normal component, the streamwise variation process of the convection rate corresponds to that of the fluctuating velocity. In the linear region the stations where the convection rates begin to decrease are x/h = 3 and 2 in the stationary and both oscillating states, respectively.

Next, the production rates in the temporal fluctuation energy and Reynolds shear stress are considered. The maximum values of the dominant production rates in the distribution in *y*-direction of $\overline{u^2}/2$, $\overline{v^2}/2$ and $\overline{uv}$ are shown in Figs. 13, 14 and 15, respectively. They are also compared with the temporally fluctuating velocities and Reynolds shear stress in Figs. 6, 7 and 9. In Fig. 13, the production rate based on the gradient of the mean velocity in the *x*-direction is also shown in the stationary state as an example. The rate increases after the disappearance of the

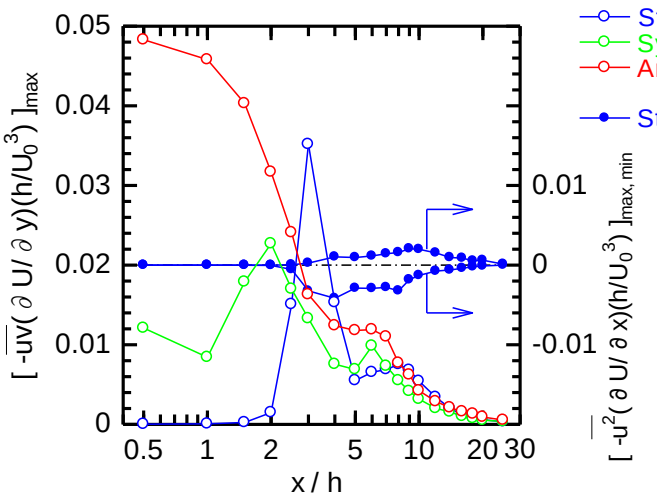

Fig. 13 Streamwise variation of maximum values of temporal fluctuation energy production rates in the streamwise component

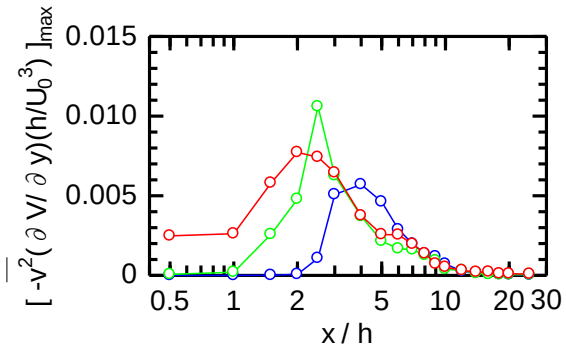

Fig. 14 Streamwise variation of maximum values of temporal fluctuation energy production rates in the normal component

potential core, though the value is not comparable to that based on the gradient in the *y*-direction. Therefore, in what follows, all production rates are based on the gradient in the *y*-direction.

First, the streamwise components, Fig. 6 and 13, are compared. The fluctuation energy production rates become maximum at x/h = 3, 2 and 0.5 in the stationary, symmetrical and anti-symmetrical oscillating states, respectively. Therefore, the streamwise variation is shifted more upstream due to the oscillation disturbance. In addition, the streamwise variation is shifted more upstream and is increased due to the anti-symmetrical disturbance. These tendencies almost correspond to the fluctuation from the time-averaged velocity, u'_{max}, in Fig. 6, except for the anti-symmetrical oscillating state in the region $x/h \leqq 1$. In the linear region, $x/h < 2$, the production rate in the anti-symmetrical oscillating state is larger than that in the symmetrical oscillating state as well as u'_{max} in Fig. 6. Therefore, as the fluctuation energy convection, the production contributes to the increase of the streamwise fluctuating velocity in the linear region. Moreover, although the production rates in all states take large values at almost the end of the linear region (x/h = 3 and 1.5 in the stationary and both oscillating states, respectively), they are almost zero farther downstream. Thus, the energy transfer from mean to fluctuating motions happens most in the region from the end of the linear region to a little downstream, however the transfer does not happen farther downstream.

Next, the normal components, Figs. 7 and 14, are compared. In Fig. 14, the dominant fluctuation energy production rates become maximum at x/h = 4, 2.5 and 2 in the stationary, symmetrical and anti-symmetrical oscillating states, respectively. Therefore, the streamwise variation is shifted more upstream and increases due to the oscillation disturbance. In addition, the streamwise variation is shifted more upstream due to the anti-symmetrical disturbance. These tendencies almost correspond to the fluctuation from the time-averaged velocity, v'_{max} in Fig. 7. In the linear region, $x/h < 2$, the production rate in the anti-symmetrical oscillating state is larger than that in the symmetrical oscillating state as well as v'_{max} in Fig. 7. Therefore, as the fluctuation energy convection, the production contributes to the increase of the normal fluctuating velocity in the linear region. Moreover, in all states the production rates become higher at almost the end of the linear region, though they are almost zero downstream. Thus, the energy transfer from mean to fluctuating motions happens most in the region from the end of the linear region to a little downstream, although the transfer does not happen farther downstream.

Finally, the Reynolds shear stress, Figs. 9 and 15, are compared. The stations of the peak of the production rate, x/h = 4, 2 and 2, in the stationary, symmetrical oscillating and anti-symmetrical oscillating states, respectively, well coincide with the first peak stations in the Reynolds shear stress. The reason of the decrease in the production rate is due to the expansion of the mixing layer as minutely discussed previously (Ichimiya, et al., 2013a). Downstream the Reynolds shear stresses increase again at x/h = 5, 4 and 4, though the production rates are still decreasing there. Therefore, the consistent increase of the streamwise fluctuating velocity may contribute the increase of the Reynolds shear stresses as previously discussed (Ichimiya, et al., 2013a). Therefore, the Reynolds shear stress is partly contributed by the fluctuation in the streamwise velocity, Fig. 6, and partly contributed by its production rate.

Here, regions where the temporally fluctuating velocity, temporal fluctuation energy convection rate and

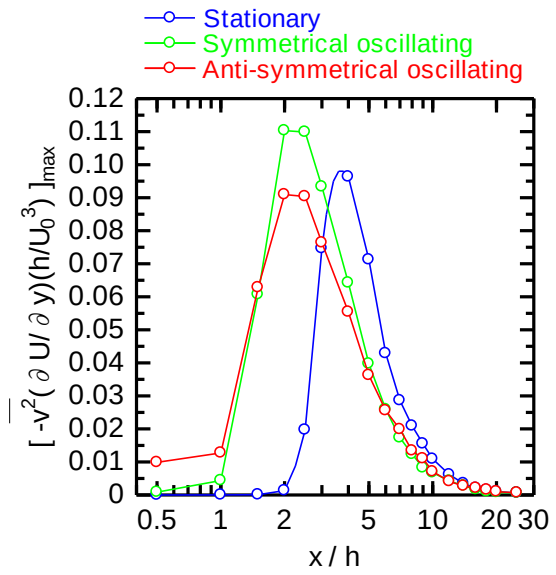

Fig. 15 Streamwise variation of maximum production rates of Reynolds shear stress component

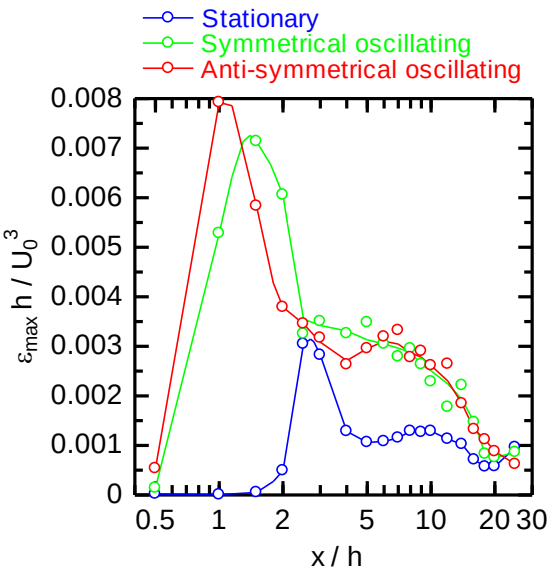

Fig. 16 Streamwise variation of maximum values of temporal fluctuation energy dissipation rates

production rate increase are compared. The streamwise component of the energy convection and production rates becomes maximum at around the end of the linear region, though the fluctuating velocity continues to increase farther downstream. Therefore, factors other than the convection and production rates might contribute to the increase in the streamwise velocity fluctuation in the nonlinear region such as the energy redistribution rate between components due to the three-dimensionalization of the fluctuation. On the other hand, convection and production rates which contribute to the normal component become maximum in the nonlinear region, and the fluctuating velocity itself becomes maximum around there. Therefore, the convection and production rates may well contribute to the increase of the normal fluctuating velocity.

Figure 16 shows the temporal fluctuation energy dissipation rate, which is an important factor as the convection and production rates. As usual, the dissipation rate was estimated from $15\nu\overline{(\partial u/\partial t)^2}/U^2$, by assuming an isotropy and frozen turbulence. As different from the production and convection rates in Figs. 11-14, the dissipation rate is for the total component, $(\overline{u^2}+\overline{v^2}+\overline{w^2})/2$. The streamwise variation of the rates in the both oscillating states shift upstream and become larger than in the stationary state. Hence, the oscillation disturbance, especially the anti-symmetrical disturbance, increases the dissipation rate.

4. Conclusions

A small amplitude and anti-symmetrical disturbance was locally created with low frequency, and then this disturbance was forced to enter a mixing layer formed at the exit of a two-dimensional nozzle. The laminar-turbulent transition in the mixing layer is investigated experimentally. The following conclusions were obtained.

(1) The oscillation disturbance promotes the disappearance of the potential core. The anti-symmetrical disturbance is more effective in the mixing and expansion of the mixing layer.

(2) Downstream, the fluctuation from the time-averaged velocity in the anti-symmetrical oscillating state is larger than in the symmetrical oscillating state due to the periodic motion.

(3) The irregular fluctuation from the phase-averaged velocity in the anti-symmetrical oscillating state is larger than in the symmetrical oscillating state. An effect of the periodic disturbance disappears in the symmetrical oscillating state downstream. On the other hand, in the anti-symmetrical oscillating state, the effect of the disturbance persists farther downstream.

(4) Initially, the linear region where the irregular fluctuation on the periodic fluctuating velocity grows exponentially. There are not any differences in the spatial growth rate between two velocity directions and among three oscillating states.

(5) In the nonlinear region, factors other than the temporal fluctuation energy convection and production rates

may contribute to the increase in velocity fluctuation in the streamwise component. On the other hand, the convection and production rates may contribute to the increase in velocity fluctuation in the normal component there.

References

Brown, G. L. and Roshko, A., On density effects and large structure in turbulent mixing layers, Journal of Fluid Mechanics, Vol. 64, Pt. 4 (1974), pp. 775–816.

Huang, L.-S. and Ho, C.-M., Small-scale transition in a plane mixing layer, Journal of Fluid Mechanics, Vol. 210 (1990), pp. 475–500.

Ichimiya, M., Kato, T. and Morimoto, T., Effect of local periodic disturbance on mixing layer at exit of two-dimensional jet, Journal of Fluid Science and Technology, Vol. 6, No. 6 (2011), pp. 887–901.

Ichimiya, M., Kamada, S., Okajima, A. and Osaki, T., Effect of local periodic disturbance on mixing layer downstream of two-dimensional jet (Spatial structure and quantitative representation of laminar-turbulent transition process), Journal of Fluid Science and Technology, Vol. 8, No. 1 (2013a), pp. 90–105.

Ichimiya, M., Miura, T. and Kamada, S., Effect of local periodic disturbance on mixing layer downstream of two-dimensional jet (Effect of amplitude and frequency of the disturbance), Transactions of the Japan Society of Mechanical Engineers, Series B, Vol. 79, No. 806 (2013b), pp. 2093–2108 (in Japanese).

Makita, H., Ohtani, H. and Ishizumi, K., Acoustic control of jet structure (1st Report, On the difference of jet structure by acoustic excitation modes), Transactions of the Japan Society of Mechanical Engineers, Series B, Vol. 54, No. 504 (1988), pp. 1938–1945 (in Japanese).

Michalke, A., On spatially growing disturbances in an inviscid shear layer, Journal of Fluid Mechanics, Vol. 23, Pt. 3 (1965), pp. 521-544.

Moore, C. J., The role of shear-layer instability waves in jet exhaust noise, Journal of Fluid Mechanics, Vol. 80, Pt. 2 (1977), pp. 321–367.

Rajaratnam, N., Turbulent Jets (1976), Elsevier.

Rotta, J. C., Turbulent boundary layers in incompressible flow, Ferri, A., Kuchemann, D. and Sterne, L. H. G. ed., Progress in Aeronautical Sciences (1962), p.43, Pergamon Press.

Sato, H., The stability and transition of a two-dimensional jet, Journal of Fluid Mechanics, Vol. 7 (1960), pp. 53–80.

Schlichting, H. and Gersten, K., Boundary-Layer Theory, 8th Revised and Enlarged ed. (2000), p.652, Springer.

Shakouchi, T., Jet Flow Engineering -Fundamentals and Application- (2004), Morikita Shuppan (in Japanese).